The Astrophysical Journal Letters, 872:L5 (6pp), 2019 February 10 https://doi.org/10.3847/2041-8213/ab01db

Crater Density Predictions for New Horizons Flyby Target 2014 MU69

Sarah Greenstreet[1,2], Brett Gladman[3], William B. McKinnon[4], J. J. Kavelaars[5], and Kelsi N. Singer[6]
[1] B612 Asteroid Institute, 20 Sunnyside Avenue, Suite 427, Mill Valley, CA 94941, USA
[2] DIRAC Center, Department of Astronomy, University of Washington, 3910 15th Avenue NE, Seattle, WA 98195, USA
[3] Department of Physics & Astronomy, 6224 Agricultural Road, University of British Columbia, Vancouver, British Columbia, Canada
[4] Department of Earth and Planetary Sciences and McDonnell Center for Space Sciences, One Brookings Drive, Washington University, St. Louis, MO 63130, USA
[5] National Research Council of Canada, Victoria, British Columbia, Canada
[6] Southwest Research Institute, 1050 Walnut Street, Suite 300, Boulder, CO 80302, USA
Received 2018 December 21; revised 2019 January 22; accepted 2019 January 25; published 2019 February 7

Abstract

In preparation for the 2019 January 1 encounter between the New Horizons spacecraft and the Kuiper Belt object 2014 MU69, we provide estimates of the expected impact crater surface density on the Kuiper Belt object. Using the observed crater fields on Charon and Pluto down to the resolution limit of the 2015 New Horizons flyby of those bodies and estimates of the orbital distribution of the crater-forming projectiles, we calculate the number of craters per unit area formed as a function of the time a surface on 2014 MU69 has been exposed to bombardment. We find that if the shallow crater size distribution from roughly 1–15 km exhibited on Pluto and Charon is indeed due to the sizes of Kuiper Belt projectiles, 2014 MU69 should exhibit a surface that is only lightly cratered below 1 km scale, despite being bombarded for ∼4 billion years. Its surface should therefore be more clearly indicative of its accretionary environment. In addition, this object may be the first observed for which the majority of the bombardment is from exogenic projectiles moving at less than or near the speed of sound in the target materials, implying morphologies more akin to secondary craters elsewhere in the solar system. Lastly, if the shallow Kuiper Belt size distribution implied from the Pluto and Charon imaging is confirmed at 2014 MU69, then we conclude that this size distribution is a preserved relic of its state ≃4.5 Gyr ago and provides a direct constraint on the planetesimal formation process itself.

Key words: Kuiper Belt objects: individual (2014 MU69) – planets and satellites: surfaces

1. Introduction

The upcoming flyby of the New Horizons spacecraft by the cold classical transneptunian object (486958) 2014 MU69 (hereafter referred to as MU69) will offer the first up-close look (sub-km resolution) of a small outer solar system body in its formation environment, and will provide the first opportunity to observe a high-resolution cratered surface of a transneptunian object (TNO) other than those in the Pluto system, imaged by New Horizons in 2015 July (Stern et al. 2015; Moore et al. 2016, 2018).[7]

The classical Kuiper Belt appears to be divided into at least two separate inclination components (Brown 2001). The "cold" classical Kuiper Belt (Kavelaars et al. 2008) contains the vast majority of the TNOs on low-eccentricity orbits *of low inclination* in the semimajor axis range $42.4 < a < 47$ au (Petit et al. 2011). The existence of large-separation TNO binaries combined with their small orbital inclinations suggests that the cold classicals represent a reservoir of the primordial protoplanetary disk beyond 40 au (Parker & Kavelaars 2010). This is the only sub-population thought to have been in place since the formation of the solar system. The low orbital inclination and eccentricity of MU69's orbit (Porter et al. 2018) place this object firmly within this region, and thus MU69 is likely to have formed at this large heliocentric distance and be the most primitive outer solar system body yet visited. There is considerable structure in the a and eccentricity (e) space of the cold population, and it is has been split (Petit et al. 2011) into a "stirred" component crossing the whole cold a range, and a much more confined "kernel" of cold objects near $a = 44$ au and $e \simeq 0.05$; MU69 is consistent with being in this kernel.

It has been postulated that the other Kuiper Belt sub-populations (characterized by broader orbital inclination distributions) formed closer to the Sun and were transplanted to their current location in the final stages of planet formation (e.g., Levison et al. 2008). The postulated 500 Myr delay in the instability in the often-cited Nice Model (Gomes et al. 2005) has been retreated from (Mann 2018); a short phase (with most of the action in $\lesssim$1% the age of the solar system) that happens during the initial planet formation epoch is now in vogue (see Nesvorný 2018 for a recent review). The desirable implantation properties for creating the Kuiper Belt structure, however, still hold even if the instability process occurs early (within a few to tens of Myr) in solar system history (Gladman et al. 2012). In the scenario in which MU69 has always been near its current orbit, a hypothetical metastable (pre-instability) phase (which was of interest for Pluto's early cratering given that Pluto is part of the metastable population) is almost irrelevant, because during the early phase the population closer to the Sun is not cratering MU69. In either case, the "hot" populations are ultimately emplaced during a relatively brief ($\lesssim$1% of the solar system's age) period in which the cold population must not be dynamically excited (e.g., Dawson & Murray-Clay 2012). While we thus concentrate our calculations on the last 4 Gyr of bombardment, we argue below that the *brief* phase in which the objects were scattered out through the Kuiper Belt, with some small fraction becoming the hot classical Kuiper Belt that we see today, cannot contribute a large ($>$ factor of 2) amount of MU69 cratering, especially given that we find that the cold populations dominate the impactor flux.

[7] The New Horizons flyby of MU69 was successful, and initial images from the close encounter have been downlinked (Stern et al. 2018).

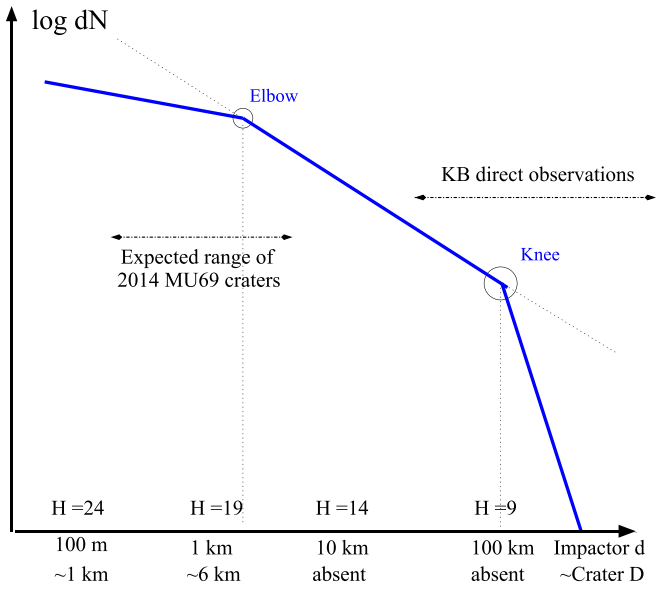

Figure 1. Cartoon schematic of the H_g-magnitude differential size distribution. The Kuiper Belt observations are well calibrated down to $H_g \approx 10$, but smaller than the knee at $H_g \sim 9$ (open circle) the size distribution flattens from a slope of $\alpha \simeq 0.8$ (which corresponds to a differential diameter power law with index 5.0; sizes not relevant to this Letter) down to a shallower $\alpha \simeq 0.4$ (which corresponds to a differential power law with index 3.0). Singer et al. (2019) find that the impactor size distribution from craters observed on Charon requires a second change to a slope of $\alpha \simeq 0.15$ (corresponding to a differential diameter power law with index 1.75) for $d \lesssim 2$ km. For reference, impactor diameters d are converted to rough MU69 crater diameters D, assuming a common impact speed of 300 m s^{-1}. It is expected that craters down to $D \approx 200$ m (created by cold-belt impactors with $d \gtrsim 20$ m) will be observable by New Horizons (Moore et al. 2018).

The crater size-frequency distributions on Pluto and Charon observed by the New Horizons spacecraft during its flyby of the Pluto system in 2015 July showed a change to a shallower size distribution at small crater sizes (Robbins et al. 2017; Singer et al. 2019). We assume that this transition is caused by a similar paucity of small impactors, and combine the derived impactor size distribution with a Kuiper Belt orbit distribution model to compute the impactor flux, impactor speed distributions, and resulting crater formation rates on MU69.

2. The Impactor Size Distribution

Calculating crater formation rates requires a knowledge of the impactor population's orbital distribution (which determines the impact probabilities and impact speed distribution) and its diameter d distribution in order to compute the scale of the resulting craters of diameter D. The differential number of objects dN as a function of absolute H-magnitude behaves locally as $dN \propto 10^{\alpha H}$, where the exponential index α is also referred to as the logarithmic "slope" (hereafter referred to simply as the slope). This corresponds to a cumulative power-law distribution in the projectile diameter with $N(>d) \propto d^{-5\alpha}$. The conversion for objects with absolute g-band magnitude H_g and scaling to an albedo p of 5% is

$$d \backsimeq 100 \text{ km} \sqrt{\frac{0.05}{p}}\ 10^{0.2(9.16-H_g)}, \quad (1)$$

where we see that $H_g = 9.16$ corresponds to 100 km. We have chosen to make a single pre-encounter crater density prediction, based on telescopic observations and the results of the New Horizons flyby of Pluto and especially Charon (the latter unaffected by aeolian or glacial processes). We use one size distribution (Figure 1) for all of the various Kuiper Belt sub-populations.[8] The steep observed Kuiper Belt size distribution for TNOs with $d > 100$ km rolls at this diameter to a "knee" size distribution, as used in Greenstreet et al. (2015, 2016); the slope $\alpha = 0.4$ below this knee extends down to another slope change at a scale that Singer et al. (2019) denote as the "elbow," visible on both Pluto and Charon. On Charon, this corresponds to a crater size of $D \approx 13$ km, which for typical Charon impact speeds implies a projectile with $d \approx 2$ km and thus $H_g \approx 17.5$. We connect the $H_g < 9.16$ population estimates from Petit et al. (2011) and Gladman et al. (2012) to the $H_g < 17.5$ scale by using a multiplicative factor of $10^{\alpha\Delta H} = 10^{((0.4*8.5)-(0.8*0.16))} \approx 1900$. Below this scale, Pluto and Charon show a very shallow crater distribution with $\alpha \simeq 0.15$,[9] and we assume that this slope is coming from the impactor size distribution and directly map it back to the projectiles. Figure 1's horizontal axis also shows the expected crater diameter caused by a typical cold-population impactor striking MU69 (see below). If this crater size distribution is in fact present on MU69, it will be a dramatic confirmation of a shallow Kuiper Belt size distribution in the roughly 0.1–2 km diameter range.

3. Methods

The methods for computing the current impact fluxes and cratering rates onto MU69 are identical to those in Greenstreet et al. (2015, 2016), to which we refer the reader for the details; below we only mention any deviations from the methods used in the previous paper.

3.1. Kuiper Belt Population Models

MU69 sits in the heart of the cold classical Kuiper Belt's kernel with the encounter target having $a = 44.2$ au, $e = 0.04$, and heliocentric J2000 orbital inclination $i = 2.^\circ4$ (Porter et al. 2018). We adopted the same orbital distributions and $N(H_g < 9.0)$ population estimates for the various Kuiper Belt sub-populations as before and computed the impact fluxes onto MU69. We added the population of TNOs in the 7:4 mean-motion resonance with Neptune (whose population is small and was thus not used for the Pluto/Charon analysis), because the resonant semimajor axis of $a \simeq 43.6$ au is close to MU69 and the impact probability per particle is enhanced, thus contributing a non-negligible fraction of the total impact flux onto MU69.

As in Greenstreet et al. (2015, 2016), we account for the slow decay of each projectile sub-population over the last 4 Gyr when we compute the total impact flux. For the 7:4 resonance, we adopt the same decay as for the 2:1 objects found in Tiscareno & Malhotra (2009). These enhancements back in time are modest except for the scattering TNO population, but

[8] Greenstreet et al. (2015, 2016) also used a differential size distribution with a divot at $H_g = 9.0$, which would drop the number of expected craters on MU69 by a factor of 6 (at all sizes).

[9] Slopes are taken directly from crater differential distributions on Charon that vary as $D^{-1.7}$ to $D^{-1.8}$, which correspond to $\alpha = 0.14$–0.16 (Singer et al. 2019).

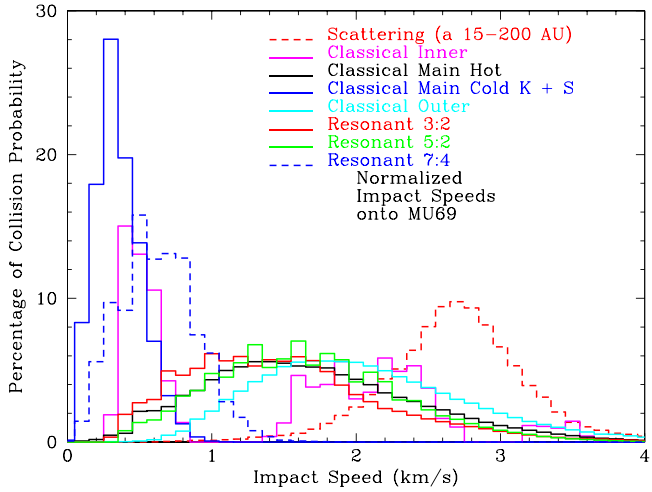

Figure 2. Impact velocity spectrum onto MU69 for each Kuiper Belt sub-population. Each sub-population's distribution is separately normalized. The cold main classical impact velocity distribution includes both the stirred and kernel sub-components, because their speed distributions are similar. The bimodal nature of the (nearly negligible) inner classical belt is due to a gap in that population's orbital inclination distribution (Petit et al. 2011). Almost all impactors on MU69 are traveling at less than the speed of sound in coherent water ice.

we show below that this population is only a tiny contributor to MU69 cratering.

3.2. Öpik Collision Probability Code

The Öpik collision probability code used in this study is the same as used previously, with the only change being the new target body. MU69's gravitational focusing is negligible, but is included. Unlike Pluto, 2014 MU69 is neither located within a mean-motion resonance nor is it undergoing Kozai oscillations. It was thus not necessary to provide a correction factor to the collision probabilities provided by the Öpik collision probability code to take into account how the dynamics allowed Pluto to avoid orbital intersections with some portions of some sub-populations. Our code provides the impact probabilities for the ensemble of objects in each orbit and the probability-weighted impact speed distribution onto MU69.

The impact speed distribution is remarkable (Figure 2). Essentially all impacts onto MU69 are at less than the $\sim$4 km s^{-1} p-wave speed in solid water ice (Vogt et al. 2008); thus, if MU69 is a coherent body, these impacts are subsonic, where the crater scaling laws are less well established (see discussion below and in Singer et al. 2013). The most extreme behavior is that, because of their similar orbits to MU69, the cold classicals have tiny impact speeds, peaking around only 300 m s^{-1}. This is similar to the p-wave speed in unconsolidated sands or porous aggregates—arguably better structural analogs to MU69's surface.[10] While such speeds are well above MU69's escape speed, they are essentially unknown for primary projectiles in the solar system and would only be seen elsewhere in the context of non-escaping, secondary projectiles. Figure 2 shows that the 7:4 resonant objects have a range of encounter speeds including serendipitous close encounters with MU69 at similarly low velocities due to their very similar semimajor axes. Unsurprisingly the scattering objects, which have large semimajor axes, peak at the highest impact velocity ($\approx$3 km s^{-1}) of the sub-populations. The remaining sub-populations peak at similar impact speeds near $\approx$1.5 km s^{-1}.

3.3. Impact Rates Onto MU69

Table 1 shows the calculated Öpik collision probabilities (/yr/TNO) onto MU69 for each Kuiper Belt sub-population (this collision probability is independent of the projectile size). This is converted to an impact rate by multiplying by the estimated corresponding population at some scale. To pick a single number, we have chosen to tabulate the rate of projectiles of the size scale of the elbow or larger ($H_g < 17.5$ or $d \gtrsim 2$ km). This reveals that the current impact rate is dominated by the three components of the main classical belt, which together supply $(10 + 58 + 18) = 86\%$ of the projectiles that have struck MU69 over the last 4 Gyr. The total impact rate of projectiles larger than the elbow is (perhaps surprisingly) low at only 0.017/Gyr; it is thus likely that over the entire post-accretionary bombardment history no projectile with $d \gtrsim 1$ km has struck MU69 (we assume an effective target radius of 10 km). We thus predict that large craters will be rare or absent; we quantify this below. The impact flux from impactors smaller than the elbow will of course be larger due to their increasing numbers as diameters drop, but with a shallow slope they do not become numerous quickly. Our calculations of crater production that follow perform the full integration over the size and speed distributions, and are thus better than quoting a single number.

Another remarkable result shown in Table 1 is that the scattering population is a fractionally negligible addition to the impact rate. The resonant populations are each small contributors. The large 3:2 population (which was the most important of the sub-populations for Pluto cratering) has a low impact probability per particle due to the large mutual orbital inclination with MU69. The enhancement of the 7:4 population (by about a factor of two per particle) is evident, but the four most important resonant sources together provide $\approx$10% of the impactor flux. The classical inner population is essentially negligible because many of its members do not intersect the MU69 orbit. Finally, the population of non-resonant TNOs with semimajor axes beyond the 2:1 resonance (the "Classical Outer" population) contributes about 9% of the impactors; this population has many orbits with perihelion just inside MU69's perihelion and, as Figure 2 shows, these impactors have median impact speeds $U \sim 2$ km s^{-1}.

Our derived impact fluxes (assuming an effective spherical radius of $r \approx 10$ km), when expressed as impacts per year per km^2 of target, are about twice that onto Pluto, reflecting the higher spatial density of the MU69 environment. This relative flux is in agreement with other estimates, which also conclude that the cold classicals should provide $\sim$80% of the impacts (Y. JeongAhn 2018, private communication).

3.4. Cratering Rates onto MU69

For the purposes of this Letter, we assume that MU69 is an unconsolidated, low-density body. We convert between crater

[10] P-wave speeds of a few hundred m s^{-1} or less are in fact likely for MU69, given its likely comet-like composition, porosity, and the known (pressure)$^{0.5}$ dependence of sound speeds in unconsolidated sand (Lambe & Whitman 1969).

Table 1
Öpik Collision Probability Calculations, $d \gtrsim 2$ km Impact Rates, and $D > 1$ km Cratering Rates onto MU69 for each Kuiper Belt Sub-population

Kuiper Belt Sub-population Type	$H_g < 17.5$ Population Estimate	Öpik Impact Probability (/yr/TNO)	$d \gtrsim 2$ km Impact Rate (/Gyr)	% of Total Impact Rate	$D > 1$ km Cratering Rate (/Gyr)	% of Total Cratering Rate
Scattering Objects (15 au $\leqslant a \leqslant$ 200 au)	2.0e7	3.4e-21	6.8e-5	0.4	7.3e-3	0.7
Scattering Objects ($a >$ 200 au)	1.8e8	1.0e-22	1.8e-5	0.1	2.1e-3	0.2
Classical Inner	5.5e6	5.6e-22	3.1e-6	0.0002	2.6e-4	0.0002
Classical Main H	6.5e7	2.4e-20	1.6e-3	**9.5**	1.4e-1	**13.2**
Classical Main S	1.4e8	7.0e-20	9.8e-3	**58.0**	5.4e-1	**50.7**
Classical Main K	3.8e7	7.8e-20	3.0e-3	**17.8**	1.6e-1	**15.0**
Classical Outer	1.5e8	6.8e-21	1.0e-3	5.9	9.9e-2	9.3
Resonant 3:2	2.5e7	2.7e-20	6.8e-4	4.0	5.8e-2	5.4
Resonant 2:1	7.0e6	2.3e-20	1.6e-4	0.9	1.4e-2	1.4
Resonant 5:2	2.3e7	1.2e-20	2.8e-4	1.7	2.6e-2	2.4
Resonant 7:4	5.5e6	5.0e-20	2.8e-4	1.7	1.8e-2	1.7
Total			**0.017**	**100.0**	**1.1**	**100.0**

Note. Classical main H, S, and K are the hot, stirred, and kernel sub-populations, respectively; combined these sub-populations provide ≈86% of the impactor flux onto MU69 over the past 4 Gyr. Population estimates are for $H_g < 17.5$ (diameter $d \gtrsim 2$ km, for a g-band albedo $p = 5\%$), which is the location of the elbow (Singer et al. 2019). Current impact probabilities are (/yr/object). Impact rates are (/Gyr) and determined using the number of $H_g < 17.5$ objects in each sub-population assuming an effective target radius near 10 km (the stellar occultation silhouette is 20 × 35 km, but irregular (Moore et al. 2018)). Cratering rates for $D > 1$ km are (/Gyr) of bombardment.

diameters D and projectile diameter d via

$$D = 8.9\left(\frac{U^2_{\mathrm{km\,s^{-1}}}}{g_{\mathrm{cm\,s^{-2}}}}\right)^{0.170}\left(\frac{\delta}{\rho}\right)^{0.333} d_{\mathrm{km}}^{0.830}\ \mathrm{km} \qquad (2)$$

where U is the impact velocity (in km s^{-1}), d is the impactor diameter, and the gravitational acceleration on the surface of MU69 is $g \approx 0.3$ cm s^{-2}. We assume both impactor δ and target ρ (at surface) densities are $\delta = \rho = 1.0$ g cm^{-3}, although the value is unimportant as long as they are similar.

The coefficients in Equation (2) are appropriate to dry unconsolidated sand or regolith in the gravity regime (Singer et al. 2013), and are based on well-established scaling from laboratory and numerical simulations (Holsapple 1993; Housen & Holsapple 2011; Greenstreet et al. 2015, 2016; Singer et al. 2019). This procedure should provide a reasonably accurate estimate of crater size (to within ±50%) for the material model assumed, provided that neither the impact speed nor the cratering efficiency (excavated crater mass/impactor mass) are too low. Well-defined secondary craters are seen on icy satellites for speeds down to ≈200 m s^{-1} or less (Bierhaus & Schenk 2010; Bierhaus et al. 2012; Singer et al. 2013), so we anticipate that most TNO impacts onto MU69 will form craters; the lowest-speed impactors should be accretionary, however, not crater-forming. Despite the difference of physical regime, Equation (2) gives quite similar results to those obtained if we use the scaling law in Greenstreet et al. (2015) appropriate for non-porous coherent surfaces; when propagated through the entire analysis, the resulting crater densities presented below are nearly identical.[11] Thus, uncertainties in the scaling law are of lesser consequence compared to the much larger uncertainties that we expect to arise because of the sparse crater statistics.

First note that for the tiny $U \simeq 0.3$ km s^{-1}, craters are only $D \simeq 6$ km for a $d = 1$ km projectile, and thus the crater/projectile ratio is somewhat smaller than the typical 10–20 common elsewhere in the solar system. By integrating the crater production over all speeds of all sub-populations, we derive the crater production rates shown in Figure 3 for various bombardment timescales.

Although a single number is of limited utility, Table 1 also lists the rate of production of impact craters larger than an arbitrarily chosen size of $D > 1$ km from each projectile sub-population. This crater formation rate is low. Accounting for all the projectiles, the expectation is a modest five craters with $D > 1$ km on MU69 after bombardment for the solar system's age. Because of the low impact speeds from the cold classical sources, their dominance is somewhat diminished in terms of the fraction of the crater production above a given D limit, as their craters are smaller than those produced by the higher-speed populations; nonetheless, the cold population still manages to contribute 66% of the $D > 1$ km crater production.

Figure 3 provides a much more complete view of our results in the form of predicted cumulative crater density curves for several bombardment durations (that is, ages since a surface was last reset by geological or accretional processes). The horizontal line corresponds to one crater on the surface. The conclusion is dramatic: MU69 should be lightly cratered at all sizes, including near the resolution limit, for despite extremely low gravity on MU69, the paucity of small projectiles and their slow impact speeds produce few craters with $D > 200$ m. Even more spectacularly, given that the surface area of MU69 is only ∼1000–2000 km^2, the 4 Gyr bombardment predicts only

[11] Note added in revision: qualitatively similar results are obtained using gravity regime scaling for highly porous surfaces (Housen et al. 2018).

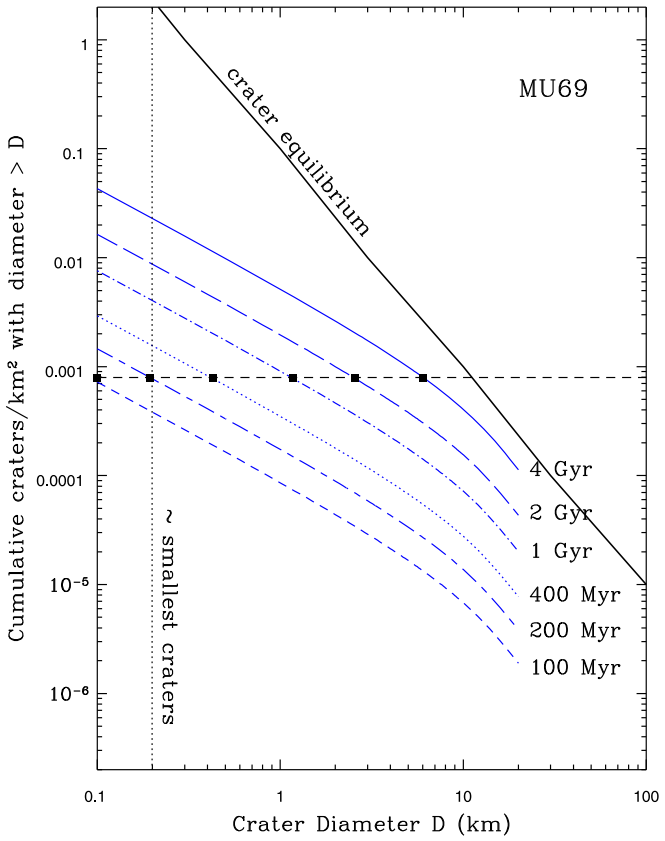

Figure 3. Logarithm of crater density (# craters/km^2) larger than a given crater diameter D on MU69's surface vs. the logarithm of the crater diameter for an impactor size distribution with a both a knee (not visible in this plot) and elbow (shown as the gradual slope change near $D \approx 10$ km) at various surface ages. The solid black line is the crater equilibrium curve from Melosh (1989). The horizontal line at $\approx 10^{-3}$ corresponds to 1 crater/MU69 surface (for a sphere of 10 km effective radius), and the vertical line is an estimate for the smallest craters that should be clearly visible in the best MU69 images. The black squares at the 1 crater/MU69 surface line correspond to the black squares in Figure 4. The change in slope at $D \approx 10$ km corresponds to the elbow break in the impactor size distribution, but will not be visible in the crater data; note that this change is gradual because of the large fractional spread in impact speeds U present.

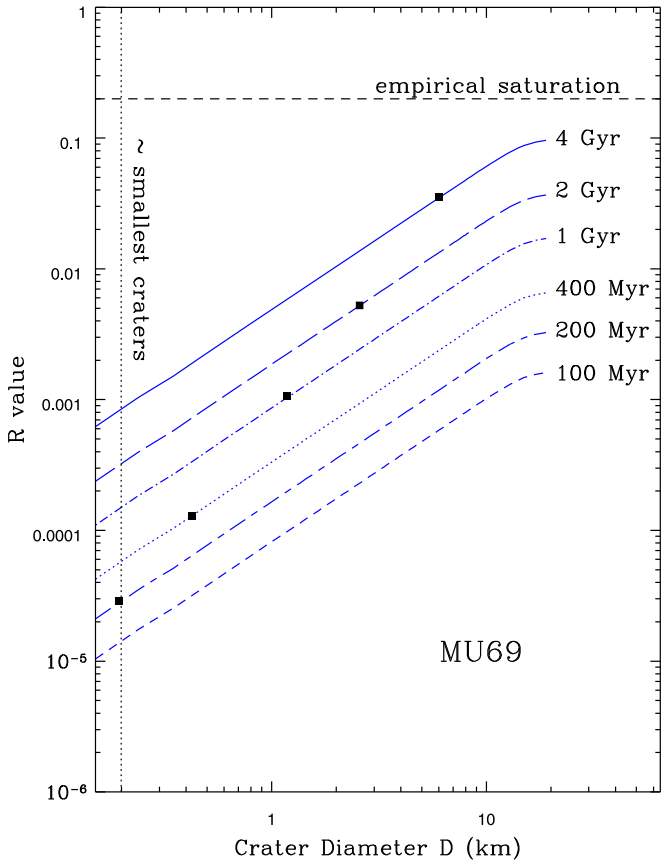

Figure 4. Relative crater frequency plot of the same information in Figure 3. The black squares correspond to 1 crater/MU69 surface on the cumulative plot (Figure 3), so craters larger than the dots will likely not be visible on MU69's post-accretionary terrains (of different ages), except by statistical fluctuation. The fact that R values rise for increasing D is due to the relatively shallow projectile size distribution implied by the Pluto/Charon surfaces. Assuming MU69 preserves the craters integrated over all of solar system history, this level of cratering in the visible portion will be sparse statistically.

$\sim$25–50 craters to be above the best-case $\sim$200 m resolution limit of MU69 (for $D > 1$ km crater estimates, see Table 1), and note that only half of the body will be imaged at this highest resolution. As long as craters are visible, however, this predicted level of cratering would provide strong confirmation that the paucity of Pluto/Charon craters smaller than the elbow scale (at crater $D < 13$ km for Pluto/Charon or impactor $d \lesssim 2$ km) is indeed a feature of the projectile size distribution. At the large end, bombardment over the entire age of the solar system will on average provide a crater with a maximum diameter of order 6 km (noting that larger craters are possible due to Poisson statistics).

Figure 4 displays our results in "R-plot" formulation, which can be thought of as roughly the fraction of the surface covered in craters at each crater scale D. The rise in R-value with increasing diameter over the visible range would be very characteristic of the projectile population derived from the Pluto/Charon crater data. If the crater counts do indeed match these predicted values, it would strongly argue that the current Kuiper Belt size distribution is extremely shallow in the $d \lesssim 2$ km diameter range probed by the MU69 (craters down to $D \approx 200$ m) and Pluto-Charon (craters with $D \lesssim 13$ km) crater counts. This would then offer the strong possibility that the current Kuiper Belt retains the primordial planetesimal-building size distribution.

4. Discussion and Conclusion

Based on the above results, we conclude that bombardment over the entire age of the solar system is insufficient to more than modestly crater 2014 MU69 near the expected resolution limit of New Horizons imagery. That is, if during MU69's formation process accretion activity was sufficient to erase any craters that may have been acquired during its assembly (if any), MU69 will be modestly cratered today. It would thus be incorrect to conclude that a lightly cratered surface implies that MU69's surface has been recently reset (or more extremely, that MU69 has been recently created as a collisional reassembly or fragment from a larger TNO (e.g., Jutzi & Benz 2017). Charon's extensive cryovolcanic plain (informally named Vulcan Planitia) is an example of this; it is unsaturated and the observed crater densities correspond to those expected from bombardment for $\approx$4 billion years (Stern et al. 2015; Moore et al. 2016; Singer et al. 2019).

Because of this light cratering, MU69 exists in an environment very different from main-belt asteroids of comparable ($\sim$10 km) size. The latter are thought to essentially

all be fragments produced after the accretionary epoch, and thus are not "primordial" objects directly (Bottke et al. 2015). In contrast, MU69 will now look very much like it did at its formation epoch (in the sense that impact processes have neither made global structural changes to the body nor even greatly affected more than a modest fraction of the surface). Despite MU69's low gravity, even the largest craters that form are unlikely to provide enough distant ejecta to erase 200 m craters; ejecta dispersal will be even more limited if MU69 is very porous, as seen at asteroid Mathilde (Veverka et al. 1999).

Looking beyond the values of the crater densities themselves, no solar system body has ever been studied where the majority of the primary cratering is from low-velocity (<1 km s^{-1}), potentially subsonic projectiles. This could result in craters with lowered depth/diameter ratios as seen for secondary craters (e.g., Bierhaus & Schenk 2010), and perhaps produce a morphologically visible difference between craters formed by impactors from the cold classical population versus those that tend to be in the 3–4 km s^{-1} range. Seeing such differences will require well-resolved craters, which we expect to be modest in number even in the best MU69 images. For the slowest impact speeds, we do not expect crater formation at all, but rather accretion of the impactor material, either as coherent mounds or dispersed debris fields ("paintball" patterns). In principle these speed differences might be able to help distinguish between craters (or other features) formed by cold classical (kernel or stirred) impactors versus those from the other sub-populations.

The uncertainty in the details of the dynamical state of the early outer solar system is only a small concern to our interpretation, due to the dominance of the cold component's impactors. Under a scenario that all the hot populations were 100–200 times more populous for a brief (~20–50 Myr) interval of solar system history (and a rapid decay during the interval is likely), this would still only double hot-population contributions to the cratering rate; Table 1 shows that even in this case the cold classical projectiles still dominate and the total cratering only rises by a few tens of percent. This is insufficient to qualitatively alter our conclusions that MU69 will be dominated by low-velocity, possibly subsonic projectiles and modestly cratered. If the object is heavily cratered, our interpretation would be that this is a crater population preserved from the initial assembly epoch of MU69 itself during the phase in which it accreted from smaller components.

Lastly, and most exciting, if the crater density and diameter distribution are consistent with bombardment over the age of the solar system by the projectile distribution that we derive based on the Pluto and Charon cratering results, this will serve as corroboration, if not convincing proof, of a very shallow sub-km size distribution in the Kuiper Belt itself (or, at least, in the cold population which dominates the MU69 crater production rate). Although Singer et al. (2019) already argue against the idea that surface geological processes on Pluto, and especially Charon, could create the shallow size distribution near and below the elbow scale (a crater size distribution that is similar across a variety of terrains on both bodies), such crater degradation processes would be extremely unlikely to work in the same way on tiny MU69. A signature with crater R values ~0.001–0.01 that are increasing as one moves to larger crater diameters would confirm that the elbow and its slope as seen on Pluto/Charon are due to a transition to a shallow projectile size distribution. If so, then not only is MU69 and its surface in a largely primordial state, but the size distribution of the projectiles themselves is also a largely unevolved relic of the formation epoch. This unusual state is possible because the $\alpha \simeq 0.15$ distribution is so shallow that there are not enough projectiles to disrupt the rapidly shrinking targets as one moves down the size distribution (Singer et al. 2019). The current Kuiper Belt size distribution (at least of the cold population) would then be that which planetesimal accretion models would have to create, and the cratering record preserved on the already-imaged objects is directly providing constraints on the planet-building process.

We thank an anonymous referee for suggested improvements to the manuscript. S. Greenstreet acknowledges support from the B612 Asteroid Institute. B. Gladman acknowledges support from the Canadian Natural Sciences and Engineering Research Council. W.B. McKinnon, J.J. Kavelaars, and K.N. Singer acknowledge support from the New Horizons project.

ORCID iDs

Sarah Greenstreet https://orcid.org/0000-0002-4439-1539
Brett Gladman https://orcid.org/0000-0002-0283-2260
William B. McKinnon https://orcid.org/0000-0002-4131-6568
J. J. Kavelaars https://orcid.org/0000-0001-7032-5255
Kelsi N. Singer https://orcid.org/0000-0003-3045-8445

References

Bierhaus, E. B., Dones, L., Alvarellos, J. L., & Zahnle, K. 2012, Icar, 218, 602
Bierhaus, E. B., & Schenk, P. M. 2010, JGR, 115, 12004
Bottke, W. F., Brož, M., O'Brien, D. P., et al. 2015, in Asteroids IV, ed. P. Michel, F. E. DeMeo, & W. F. Bottke (Tucson, AZ: Univ. Arizona Press), 701
Brown, M. E. 2001, AJ, 121, 2804
Dawson, R. I., & Murray-Clay, R. 2012, ApJ, 750, 43
Gladman, B., Lawler, S. M., Petit, J. M., et al. 2012, AJ, 144, 23
Gomes, R., Levison, H. F., Tsiganis, K., & Morbidelli, A. 2005, Natur, 435, 466
Greenstreet, S., Gladman, B., & McKinnon, W. B. 2015, Icar, 258, 267
Greenstreet, S, Gladman, B., & McKinnon, W. B. 2016, Icar, 274, 366
Holsapple, K. A. 1993, AREPS, 21, 333
Housen, K. R., & Holsapple, K. A. 2011, Icar, 211, 856
Housen, K. R., Sweet, W. J., & Holsapple, K. A. 2018, Icar, 300, 72
Jutzi, M., & Benz, W. 2017, A&A, 597, A62
Kavelaars, J., Jones, L., Gladman, B., et al. 2008, in The Solar System Beyond Neptune, ed. M. A. Barucci et al. (Tucson, AZ: Univ. Arizona Press), 59
Lambe, T. W., & Whitman, R. V. 1969, Soil Mechanics (1st ed.; New York: Wiley)
Levison, H. F., Morbidelli, A., Van Laerhoven, C., et al. 2008, Icar, 196, 258
Mann, A. 2018, Natur, 553, 393
Melosh, H. J. 1989, Impact Cratering: A Geologic Process (1st ed.; New York: Oxford Univ. Press)
Moore, J. M., McKinnon, W. B., Spencer, J. R., et al. 2016, Sci, 351, 1284
Moore, J. M., McKinnon, W. B., Spencer, J. R., et al. 2018, Icar, 246, 65
Nesvorný, D. 2018, ARA&A, 56, 137
Parker, A. H., & Kavelaars, J. J. 2010, ApJL, 722, L204
Petit, J. M., Kavelaars, J. J., Gladman, B. J., et al. 2011, AJ, 142, 131
Porter, S. B., Buie, M. W., Parker, A. H., et al. 2018, AJ, 156, 20
Robbins, S. J., Singer, K. N., Bray, V. J., et al. 2017, Icar, 287, 187
Singer, K. N., McKinnon, W. B., Gladman, B., et al. 2019, Sci, in press
Singer, K. N., McKinnon, W. B., & Nowicki, L. T. 2013, Icar, 226, 865
Stern, S. A., Bagenal, F., Ennico, K., et al. 2015, Sci, 350, 1815
Stern, S. A., Spencer, J. R., Weaver, H. A., et al. 2018, LPSC (arXiv:1901.02578v2)
Tiscareno, M., & Malhotra, R. 2009, AJ, 138, 827
Veverka, J., Thomas, P., Harch, A., et al. 1999, Icar, 140, 3
Vogt, C., Laihem, K., & Wiebusch, C. 2008, ASAJ, 124, 3613